Published online 11 August 2015

Nucleic Acids Research, 2015, Vol. 43, No. 17 ***8601–8613***
doi: 10.1093/nar/gkv821

Structural basis for selective targeting of leishmanial ribosomes: aminoglycoside derivatives as promising therapeutics

Moran Shalev[1,2], Haim Rozenberg[2], Boris Smolkin[1], Abedelmajeed Nasereddin[3], Dmitry Kopelyanskiy[3], Valery Belakhov[1], Thomas Schrepfer[4], Jochen Schacht[4], Charles L. Jaffe[3], Noam Adir[1] and Timor Baasov[1,*]

[1]Schulich Faculty of Chemistry, Technion—Israel Institute of Technology, Haifa, Israel, [2]Department of Structural Biology, Faculty of Chemistry, Weizmann Institute of Science, Rehovot, Israel, [3]Department of Microbiology and Molecular Genetics, IMRIC, Hebrew University-Hadassah Medical School, Jerusalem, Israel and [4]Kresge Hearing Research Institute, Department of Otolaryngology, University of Michigan Medical School, Ann Arbor, Michigan, USA

Received June 02, 2015; Revised July 24, 2015; Accepted August 01, 2015

ABSTRACT

Leishmaniasis comprises an array of diseases caused by pathogenic species of *Leishmania*, resulting in a spectrum of mild to life-threatening pathologies. Currently available therapies for leishmaniasis include a limited selection of drugs. This coupled with the rather fast emergence of parasite resistance, presents a dire public health concern. Paromomycin (PAR), a broad-spectrum aminoglycoside antibiotic, has been shown in recent years to be highly efficient in treating visceral leishmaniasis (VL)––the life-threatening form of the disease. While much focus has been given to exploration of PAR activities in bacteria, its mechanism of action in *Leishmania* has received relatively little scrutiny and has yet to be fully deciphered. In the present study we present an X-ray structure of PAR bound to rRNA model mimicking its leishmanial binding target, the ribosomal A-site. We also evaluate PAR inhibitory actions on leishmanial growth and ribosome function, as well as effects on auditory sensory cells, by comparing several structurally related natural and synthetic aminoglycoside derivatives. The results provide insights into the structural elements important for aminoglycoside inhibitory activities and selectivity for leishmanial cytosolic ribosomes, highlighting a novel synthetic derivative, compound 3, as a prospective therapeutic candidate for the treatment of VL.

INTRODUCTION

Leishmaniasis is the medical term used to define an array of diseases caused by pathogenic species of *Leishmania* parasites. More than 20 disease-causing parasites have been identified so far, afflicting ∼100 epidemic countries located mainly in tropical, subtropical areas and southern Europe (1). *Leishmania* parasites are transmitted to humans by the bite of infected sandflies, causing a variety of symptoms ranging from mild to life-threatening, with the most common forms being cutaneous leishmaniasis (CL), which causes self-healing skin ulcers, and visceral leishmaniasis (VL), which is lethal if untreated (1). Approximately 2 million leishmaniasis cases are reported annually of which 300 000 are of VL with over 20 000 death casualties per annum (1).

Paromomycin (PAR) is a natural aminoglycoside (AG) different from the highly potent antibacterial agent neomycin in a single NH_2-to-OH substitution at position 6′ (Figure 1). PAR has broad-spectrum antibacterial activities, but due to its strong ability to inhibit protozoan growth it is mainly used orally for the treatment of intestinal parasite infections such as amoebiasis, giardiasis and tapeworm disease (2).

PAR's therapeutic potential for the treatment of leishmaniasis was described nearly 50 years ago (3) but its therapeutic properties were not fully exploited clinically until very recently due to the low profitability of developing new drugs for treating orphan diseases. Ointments containing 15% PAR or combinations of 15% PAR with 0.5% gentamicin, a closely related AG derivative, have already been approved for the topical treatment of CL (4,5); earlier studies also highlighted the therapeutic potential of combining PAR with methylbenzethonium chloride (MBC) for topical administration in CL (6), the latter combination being sold

*To whom correspondence should be addressed. Tel: +972 4 829 2590; Fax: +972 4 8295703; Email: chtimor@techunix.technion.ac.il

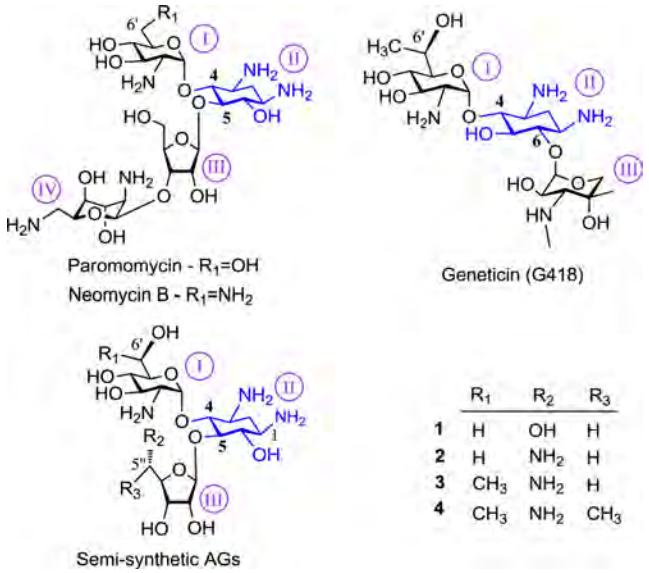

Figure 1. Chemical structures of natural and semi-synthetic AGs discussed in this study. Ring numbers are indicated in purple; the common 2-deoxystreptamine ring (ring II) is highlighted in blue and the substitution patterns for the semi-synthetic AGs are given as R_1 to R_3.

under the trade name Leshcutan (15% PAR, 12% MBC). In 2006, a phase III clinical study conducted in India demonstrated the great benefit of using PAR via intramuscular (IM) administration for the treatment of VL and as such the drug is already registered in India, Nepal and Uganda (7). In 2007, the World Health Organization (WHO) listed PAR injection for the treatment of VL as an essential medication, due to its high potency, accessibility and—most importantly—affordability in highly endemic countries (8). These publications paved the way for the ongoing registration in Bangladesh, Ethiopia, Kenya and Sudan (9). Recently, a clinical trial comparing the efficacy of liposomal amphotericin B monotherapy with PAR—liposomal amphotericin B combination therapy showed the combination treatment to be short, safe and effective; and the latter treatment was recommended in order to prevent parasite drug resistance (10).

PAR's mechanisms of action in *Leishmania* are rather obscure. Nevertheless, several lines of experimental evidence stressed the parasites' mitochondria (11), as well as cytosolic ribosomes (12–14), to be the primary targets for PAR susceptibility. Previous structural studies performed in rRNA models mimicking AGs putative binding site in cytosolic leishmanial ribosomes revealed some of the structural elements required for AG binding and activity in *Leishmania* (15). However, no comprehensive study has been performed aimed at deciphering the molecular attributes of PAR interactions with its ribosomal binding site in *Leishmania*.

The present study determined the crystal structure of PAR in complex with an RNA model, representing two leishmanial cytosolic ribosomal binding sites (A-sites) at 3.0 Å resolution. In addition, the inhibitory effects on leishmanial growth and ribosome function of a series of natural and synthetic AG derivatives, which are structurally related to PAR (Figure 1), were evaluated. These experiments demonstrated a strong correlation between the inhibition of cytosolic protein translation and the susceptibility of two highly pathogenic species of *Leishmania* parasites, implying the cytosolic ribosome as a primary target of AG action against leishmaniasis. The data presented here shed light on the structural elements important for AG inhibitory activities and selectivity to leishmanial ribosomes, highlighting several semi-synthetic derivatives, especially compound **3**, as promising therapeutic candidates for the treatment of leishmaniasis. In addition, compound **3** was found to exhibit low auditory toxicity, alleviating prominent side effect of other aminoglycosides. The high selectivity for *Leishmania* ribosomes, as well as great efficacy and better toxicity profile when compared to PAR, are highly encouraging as regards the development of new therapeutics for the treatment of VL.

MATERIALS AND METHODS

Materials

All chemical and biochemical materials used in this study, including Geneticin (G418), Paromomycin sulfate (PAR) and Amphotericin B, unless otherwise stated, were purchased from Sigma-Aldrich. The chemical synthesis of semi-synthetic aminoglycoside (AG) derivatives was performed as previously described by Baasov and coworkers (16–20). Concentrated stocks were prepared of lyophilized compounds in RNase free water or cell media; stocks were kept at −80°C. RNA oligomers were chemically synthesized by Dharmacon (GE healthcare), unprotected according to the manufacturer's instructions and purified using 20% denaturing polyacrylamide gel electrophoresis (PAGE) followed by solid phase extraction reverse-phase chromatography (Sep-Pac SPE, Waters).

Crystallization

An RNA duplex composed of two identical ssRNA oligomers (5′-UUG CGU CGU UCC GGA AAA GUC GC-3′) was used as a model representing two leishmanial A-site binding pockets. In order to ensure duplex homogeneity prior to crystallization experiments, an RNA solution containing 2 mM RNA in 100 mM sodium cacodylate (pH 7.0) and 25 mM NaCl was denaturated at 90°C for 2 min, then gradually annealed by slow cool down (∼2 h) to 37°C. The RNA-PAR complex was prepared by mixing equal volumes of annealed RNA and 4 mM PAR solutions, followed by 10 min incubation at 37°C. Crystallization experiments were set up at 20°C using the hanging-drop vapour diffusion method. Crystallization droplets were generated by mixing equal volumes (1 μl each) of the RNA/PAR complex and a crystallization solution containing 50 mM sodium cacodylate pH 7.0, 1 mM spermine tetrahydrochloride, 1% (vol/vol) 2-methyl-2,4-pentanediol (MPD), 5 mM $MgSO_4$ and 100 mM KCl. Final crystallization conditions were deduced from the optimization of an initial screen designed according to Berger et al. (21). Droplets were equilibrated against 500 μl reservoir solution containing 40% MPD. Crystals emerged after 4 days reaching their full size after 6–8 days.

Crystal handling, data collection, structure determination and refinement

Crystals were soaked in 40% MPD and flash cooled in liquid nitrogen. X-ray data were collected at ID14–4 at the European Synchrotron Radiation Facility (ESRF, Grenoble, France). Data processing performed with the XDS package (22) by merging two data sets collected from two isomorphic crystals that emerged from the same crystallization droplet. Crystallographic data statistics are summarized in Supplementary Table S1. Initial phases were determined by molecular replacement using Phaser MR as implemented in Phenix (23). The coordinates of the leishmanial A-site in complex with G418 (PDB ID code 4K32) (15) were used as a search model. Data refinement and validation have been performed using Phenix (23) and COOT (24). Structure refinement statistics are summarized in Supplementary Table S1. The solvent peaks appearing in the electron density maps were assigned as water molecules, but should rather be considered as 'unknown solvent' due the relatively low data resolution. The atomic coordinates and structure factors have been deposited in the Protein Data Bank (PDB); accession code 4ZC7. Graphical representations were made using PyMOL (25).

In vitro assays of inhibition of translation

In order to assess the susceptibility of protein translation to various AG compounds we used three different cell-free transcription-translation assays. As a representative of bacterial translation we used an *Escherichia coli* S30 cell extract supplemented with RNA polymerase and adapted for circular DNA transcription (Promega). For the eukaryotic translation inhibition assay we used S30 cell extract derived from rabbit reticulocytes supplemented with TNT® Coupled Reticulocyte Lysate Systems (Promega). The plasmids used were the pBEST*luc*™ vector (Promega) for the prokaryotic translation assay and Luciferase T7 Control DNA (Promega) for the reticulocyes; both plasmids encode for a firefly luciferase protein product. Reaction mixtures were prepared as suggested by the manufacturer except that the final reaction volume was adjusted to 10 μl to which one μl AG at the relevant concentration was added. Assays were performed in white polystyrene 96-well flat-bottom plates (Nunc). Samples were incubated for 60 min at 37°C or 30°C, respectively. Reaction was stopped by quick snap cooling followed by a five-min incubation on ice. Luciferase activity was measured immediately after the addition of 50 μl Luciferase Assay reagent (Promega) by recording the chemiluminescence signal on Tecan Infinite ® F200 microplate reader supplemented with automatic reagent injector (Tecan). *Leishmania tarentolae* inhibition of translation was tested using the *in vitro* LEXSY translation system (Jena Bioscience) supplemented with a pLEXSY-*in-vitro*^{2} vector encoding an enhanced green fluorescent protein (EGFP). Reaction mixtures (10 μl) containing various AG concentrations were prepared in black polystyrene 384-well flat-bottom (small volume) plates (Greiner) and incubated at 26°C for 120 min. GFP fluorescence was measured directly by using Tecan Infinite ® F200 microplate reader (Tecan) (λex = 488 nm; λem = 507 nm). In all cell free assays, extracts lacking the circular DNA template were used as negative control and used to calculate the fluorescence/chemiluminescence background, whereas reaction mixtures that did not contain an AG derivative were used as positive controls and were regarded as 100% translation. At least six different AG concentrations were obtained to plot each translation inhibition curve. Half maximal inhibition concentrations (IC_{50}) values were calculated from the concentration-response fitting curves of at least three independent repeats using GraFit5 software (26).

Leishmania cell culture and promastigote viability assays

Two strains of *Leishmania* were used to test *Leishmania* susceptibility to both natural and semi-synthetic AG derivatives: *Leishmania donovani* (MHOM/SD/1962/1S-Cl2d) and *Leishmania major* (MHOM/IL/2003/LRC-L1025). Promastigotes were grown in complete M199 medium (Sigma) containing 20% FCS and AG at 26°C. Compounds were initially assayed at 50 μM and then the LC_{50} was determined by serial dilution of the AGs using concentrations ranging from 0.3 to 400 μM (0.3–40 μM for G418, or 0.7–400 μM for PAR and the semi-synthetic derivatives) in complete promastigote medium. Compounds were aliqouted in triplicate (125 μl per well) to 96-well flat-bottom plates (Nunc). Promastigotes (2.0×10^6 cells per ml; 125 μl per well) were added to each well and incubated for 72 h at 26°C. The alamarBlue (AbD, Serotec) viability indicator was added (25 μl per well) and the plates were incubated for an additional 5 h, at which time the fluorescence (λex = 544 nm; λem = 590 nm) was measured in a microplate reader (Fluoroskan Ascent FL). Complete medium was used as a negative control (0% inhibition of promastigote growth). Amphotericin B (1 μM), a drug used to treat visceral leishmaniasis, was included as a positive control in each plate.

Inhibition of L. donovani amastigotes in infected THP-I macrophage cells LC_{50}

THP-1 cells in the logarithmic growth phase were incubated with 25 ng/ml phorbol 12-myristate 13-acetate (PMA) in RPMI-1640 plus 10% fetal calf serum (complete medium) for 24 h in a 5% CO_2 incubator at 37°C. Undifferentiated cells and PMA were removed by washing once with warmed RPMI-1640 and stationary-phase Ld:pSSU-int/LUC promastigotes added to the treated macrophages at a 5:1 parasite/macrophage ratio. The cells were incubated for an additional 24 h at 37°C in a 5% CO_2 incubator to allow for infection and differentiation of the parasites into intracellular amastigotes. The medium was removed and cells were washed 4–5 times with warm RPMI-1640, until no external parasites were observed by microscopic examination. Infected macrophages (iMQ) were suspended by trypanization (3–5 ml Trypsin EDTA Solution B, Biological Industries) for 2 min at 37°C after which 10–12 ml of complete medium was added. Complete iMQ release was checked by inverted microscope, and a sample (500 μl) removed, centrifuged (Cytospin Cytocentrifuge), and Geimsa stained to confirm macrophage infection. iMQs were dispensed in triplicate (100 μl/well at 5×10^5 cells/ml) into white 96-well flat bottom plates (Nunc). Drugs and compounds diluted in complete RPMI-1640 containing 1% DMSO (50 μl/well)

were added to the iMQs and the cultures incubated for 48 h (37°C, 5% CO_2). Cells were lysed by the addition of Bright-Glo Luciferase Assay substrate (100 μl/well, Promega) and the luminescence measured immediately using a microplate reader (Fluoroskan Ascent FL). Complete medium both with and without DMSO was used as negative controls (0% inhibition). Amphotericin B (1 μM) was included as a positive control on each plate and gave >90% decrease in intracellular amastigotes.

In-Silico ligand binding

Flexible docking simulations were performed using Autodock Vina version 1.1.2 1 (27). RNA coordinates were extracted from the PAR-Leish structure (PDB code 4ZC7) following removal of the solvent and ligand molecules. The ligand molecules, namely compounds **1–4**, were prepared by manipulating PAR coordinates derived from the PDB entry 1J7T using the auto-builder function implemented in PyMol (25). Hydrogen atoms were added to both the RNA and the ligands using PyMol, the Gesteiger atomic partial charges were later calculated using the ADT module from MGLTools 1.5.6 package (28). All rotatable bonds within the ligands were allowed to rotate freely. The grid box parameters for the docking procedures were determined according to prior docking validation experiment that was designed to test PAR binding modes to a bacterial A-site model using the PDB entry 1J7T (PAR-BACT) as a study case model. Exhaustiveness value was set to 400, possible conformer's number was limited to 20, and all other parameters were similar to those previously described by Aghdam et. al. (29). For each compound, 20 independent docking experiments were performed, resulting in a total of 400 poses (20 experiments x 20 poses). The best poses from each experiment were selected according to the binding modes of the conserved conformation of rings I and II. Poses of which the percentage of appearance was greater than 20% were taken for statistical analysis and determination of calculated free energy of binding. Graphical representation and structure analysis was performed using PyMol (25).

Toxicity assays in cochlear explants

Drugs were screened for toxicity to auditory hair cells in explants of the organ of Corti from CBA/J mice of postnatal day 2–3. The dissected tissue was placed on a collagen-coated incubation dish as a flat surface preparation in 1 ml of serum-free Basa Medium Eagle (Sigma Aldrich, St. Louis, MO) plus serum-free supplement (Invitrogen, Eugene, OR), 1% bovine serum albumin, 2 mM glutamine, 5 mg glucose /ml and 10 units penicillin /ml. The explants were incubated for 5 h (37°C, 5% CO_2) and an additional 1 ml of culture medium was added to submerse the explants. After 48 h of continued pre-incubation the culture medium was exchanged for new medium containing a specified concentration of the drug. Following another 72 h of incubation, the explants were washed three times with PBS, fixed overnight in 4% (v/v) paraformaldehyde at 4°C, and then permeabilized for 30 min with 0.3% (v/v) Triton X-100 in PBS. The specimens were washed three times with PBS for 10 min at room temperature and incubated with rhodamine phalloidin (1:100; Life Technologies, Eugene, OR), either for 1 h at room temperature or overnight at 4°C. Following several rinses with PBS, the explants were mounted on microscope slides with Fluoro-Gel (Electron Microscopy Sciences, Hatfield, PA) and imaged on a Leica SP5 Confocal TCS Microscope (Leica, Wetzlar, Germany). Hair cells were identified by phalloidin- staining of their stereociliary bundles and circumferential F-actin rings (see Figure 6C). Their presence or absence was quantified using a 50x oil immersion objective on an epifluorescence Leitz Orthoplan microscope (Leica, Wetzlar, Germany), equipped with a calibrated scale (0.19 mm) superimposed on the field of view. All rows of hair cells were oriented longitudinally within each frame and counted from the apex of the cochlea to its base. Cell counts were entered in a computer program and compared to a normative database (KHRI Cytocochleogram, version 3.0.6, Kresge Hearing Research Institute, University of Michigan, Ann Arbor, MI, USA) and are reported as percent hair cell loss averaged over the entire length of the explant.

Assessment of auditory toxicity *in-vivo*

Hartley male guinea pigs of initially about 200 g (Charles River Laboratories, Wilmington, MA) had free access to water and food and were acclimated for one week before experiments. Auditory thresholds at 12 kHz and 32 kHz were recorded by Auditory Brainstem Response (ABR) in an electrically and acoustically shielded chamber (Acoustic Systems, Austin, TX). Animals were anesthetized with an intramuscular injection of 50 mg ketamine and 5–10 mg xylazine/kg body weight and body temperature was maintained through the use of heating pads and heat lamps. For recordings, sub-dermal needle electrodes were placed at vertex (active), the test ear (reference) and the contralateral ear pinnae (ground). Test tones were delivered through an EC1 driver with the speculum placed just inside the external auditory canal. Stimuli were generated and ABR traces recorded with Tucker Davis Technologies System III hardware and SigGen/BioSig software (TDT, Alachua, FL). Stimuli consisted of 15 ms tone bursts, with 1 ms rise/fall times, at a rate of 10 per s, presented in 10 dB steps, with 5 dB steps near threshold; up to 1024 ABR responses were averaged for each stimulus. Thresholds were interpolated between the lowest stimulus level yielding a response and the level 5 dB lower not yielding a response.

Drugs were administered beginning one week after the baseline ABR. They were injected s.c. once daily for 14 d at dosages indicated in the figure legends; saline injections of the same volume served as controls. Three weeks after the end of drug treatment, ABR measurements were repeated and individual differences in thresholds calculated as drug-induced threshold shift.

RESULTS AND DISCUSSION

Structural overview of PAR binding modes to the leishmanial A-site

The structure of PAR bound to an RNA duplex representing two *Leishmania* ribosomal A-sites was elucidated

by X-ray crystallography at 3.0Å resolution (Supplementary Table S1, Figure 2). Similar RNA models have been used extensively for the exploration of AG interactions with ribosomal A-sites belonging to both prokaryotic and eukaryotic systems (30–38). Such minimal model was based on previous findings that these constructs mimic accurately (36,39) the A-site geometry in all available high-resolution structures of bacterial ribosomes in complex with several AG derivatives; therefore it was suggested that the model could be used for the structural investigations of AG binding pockets within ribosomes.

The crystals from co-crystallization experiments of PAR with the RNA duplex (PAR-Leish) contain two nearly symmetry-related RNA molecules in the asymmetric unit (Supplementary Table S1; Figure 2A, Molecules A and B); each molecule contains two putative leishmanial binding sites. Interestingly, in contrast to previous structural studies reporting the interaction pattern of AGs with similar leishmanial double A-site models (15), only a single A-site is occupied per molecule in the PAR-Leish structure (Figure 2). In an earlier report, both binding sites were occupied by ligand molecules and shared an identical geometry upon ligand binding. The bound conformation of the PAR-Leish structure greatly differs from the unbound conformation; these conformational differences reveal that structural rearrangements occur upon ligand binding. Observing both the unoccupied and occupied binding sites is indeed fortuitous since such differences would be difficult to predict using computational methods.

PAR, like other derivatives belonging to the AG family, contains a conserved aminocyclitol—2-deoxystreptamine (2-DOS) ring (ring II) that is di-substituted at positions 4 and 5 with modified aminosugars moieties (Figure 1). Hence, it did not come as a great surprise that the 'bound' conformation of the PAR-Leish structure highly resembles the previously reported structure of geneticin (G418), a structurally related AG, bound to a leishmanial A-site model (G418-Leish) (Figure 3B) (15). In the bound conformation, the AG occupies the internal core of the rRNA binding pocket, stabilizing the two evolutionarily conserved adenine residues, A1492 and A1493 (*E. coli* numbering), in a fully flipped-out orientation (Figure 3A). A similar A-site conformation is also observed in bacterial ribosomes upon binding of cognate tRNA molecules and as such, the two highly conserved adenine residues were postulated to serve as a molecular switch that modulates the translation elongation upon tRNA selection (40–42). The flipped-out conformation was designated as an 'ON-state' conformation since it is considered to signal the continuation of the elongation process at the ribosome upon cognate tRNA recognition (43,44).

In contrast to the 'bound' conformation, the 'un-bound' binding pocket geometry is much more flexible and therefore vastly different (Figure 3E); lacking the steric hindrance caused by the ligand, A1492 is free to interact with G1408 in a non-canonical manner *via* their Watson–Crick–Watson–Crick interfaces. As a result, A1492 is oriented towards the inner part of the helical core at about 180 degrees in regards to the 'bound' state (Figure 3F). These interactions leave A1493 to be 'un-paired', and in the absence of a ligand molecule stabilizing it in a flipped-out conformation this residue is demonstrating high flexibility with a rather weak electron density signal (for those reasons we chose not to include A1493 on our X-ray model representation, Supplementary Figure SI). A similar conformation was also earlier reported in vacant bacterial ribosomes, and in contrast to the fully flipped-out conformation was designated as an 'OFF-state conformation (43,44).

A detailed analysis of PAR interaction pattern within the binding pocket

Two PAR molecules are present in an asymmetric unit of the PAR-Leish structure (Figure 2, Supplementary Table S1), each bound to a different rRNA duplex. Despite resulting in the same structural rearrangements of the binding pocket, each PAR molecule demonstrates a unique binding pattern (Figure 3D). Superimposition of the two 'bound' molecules indicates that PAR rings I and II serve as a conserved anchor (Figure 3D) in which ring I is stacked upon A1491 while interacting in a 'pseudo-pair' manner with G1408 located at the opposite strand (Supplementary Figure SII). Ring II mainly interacts via electrostatics with the backbone of A1492 and A1493, stabilizing their flipped-out conformational state (Supplementary Figure SII). Similar interactions were reported for AGs sharing the same two-ring anchor with both bacterial and leishmanial binding pockets (15,36,38). These results are also supported by earlier biochemical evidence, indicating that the first two rings of PAR, also called paromamine, are considered as the minimal active unit interacting with both prokaryotic (45) and eukaryotic (18) ribosomes.

In contrast to the first two rings, the orientations of rings III and IV vastly differ between the two binding pockets. The overall conformation described for the ligand **molecule B** is highly similar to the one reported upon binding of PAR to bacterial ribosomes (Figure 3C). In contrast, ring III of **molecule A** is rotated at about 90 degrees in regards to the glycosidic bond with the 2-DOS ring (Figure 3D). These conformational alternations indicate a rather high flexibility of rings III and IV allowing the OH group at position 5" of ring III to interact with either the non-conserved residue A1491 or the highly conserved C1407 (Supplementary Figures SII and SIII). In addition, the 5" position, as implied in molecule **A**, is also located in close proximity to the non-conserved G1408. These interactions are greatly different from the previously reported structures of 4,6-disubstituted derivatives such as G418 (15,46) since ring III in 4,5-disubstituted AGs is localized at proximity to low evolutionary conserved residues that are known to differentiate between ribosome species of bacteria, protozoa and higher eukaryotes (Supplementary Figures SIII and SIV). These observations illustrate the importance of ring III and particularly position 5" in the determination of species-selectivity to AGs.

Ring IV is modelled only to the ligand bound to **molecule B**, contributing two electrostatic interactions with the oxygen atoms 1 and 2 belonging to two phosphate atoms of the highly conserved G1405 (Supplementary Figure SII, Supplementary Figure SIV). These contacts are maintained by the hydroxyl- and amino-groups at positions 2"' and 4"', respectively, and are identical to the contacts observed in

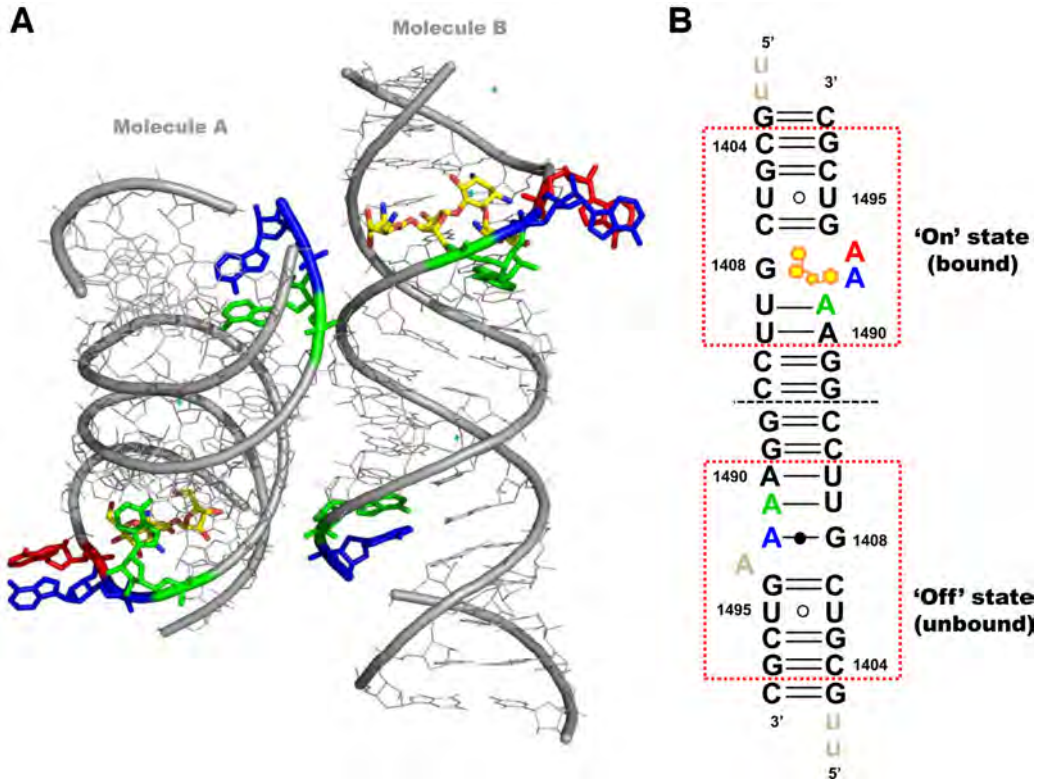

Figure 2. Three-dimensional (**A**) and two-dimensional (**B**) representations of the double A-site complexes as obtained from the X-ray crystal structures. The double A-site construct in complex with PAR contains two molecules in an asymmetric unit (molecules A and B); each represents two ribosomal binding sites (A-sites) with only one PAR (yellow) bound per RNA molecule (PDB ID code 4ZC7). The unbound conformation is vastly different from the bound conformation. The bound state represents a typical 'ON-state' conformation where A1492 (blue, according to *E. coli* numbering) and A1493 (red) are bulged out from the helical core and A1491 (green) is directed towards the inner part of the binding pocket. The unbound state represents an 'OFF-state' conformation where the adenine residues 1491 (green) and 1492 (blue) are directed towards the inner part of the helical core. In the un-bound conformation A1493 was removed from the model due to relatively low electron density resulting from high flexibility or multiple conformational alternatives within the crystal.

the structure of PAR bound to the bacterial A-site (PAR-Bact) (36). Ring IV was omitted from the ligand bound to **molecule A**, despite the fact that its presence was clearly observed at the Fo-Fc electron density maps in proximity to U1406 (Supplementary Figure SI). However, due to the unstructured shape of the 'un-modelled' electron density blob, it was impossible to definitively determine the ring orientation, and as such it was decided not to include it in the final model. The undefined shape could result from the rather low structural resolution or high ring flexibility.

In vitro evaluation of AG inhibition of translation in Leishmania: the influence of ring III 5" modifications on leishmanial ribosome selectivity

The structural results shed light on PAR binding modes to leishmanial ribosomes and highlighted ring III as a promising candidate of chemical modifications for the selective targeting of species specific ribosomes. As a first step towards the assessment of such notion we evaluated the impact of two synthetic PAR derivatives (**compounds 1–2**, Figure 1) on *Leishmania* translational machinery *in vitro*. The two compounds share a common three-ring PAR like scaffold, lacking ring IV, and differing at the identity of their 5" moiety only. The biological activity was assessed by calculating the half-maximal inhibitory concentration (IC_{50}) values of protein translation in a cell free system derived from *L. tarentolae* (Table 1).

The results indicated that compound **1**, which contains PAR rings I-III with a hydroxyl moiety at position 5", has significantly reduced inhibition potency when compared to PAR (PAR, IC_{50} - 3.9 μM; compound **1**, $IC_{50} > 20$ μM; Table 1). A similar tendency was also observed in compound's **1** ability to inhibit bacterial and higher eukaryotes ribosome translation (Table 1). The reduced potency might be explained by the loss of ring IV, hence the elimination of the highly conserved polar contacts that might be important for binding site anchoring in all ribosomal species (Supplementary Figure SIV). Interestingly, the loss of potency for the three-ring structure could be compensated by a single substitution of the 5"-OH (ring III) with a 5"-NH_2 moiety (compound **2**, IC_{50} - 3.5 μM, Table 1). A similar trend was also observed in rabbit reticulocytes translation system, but not in bacteria (Table 1). These results imply that 5" amino modified compounds show superior selective inhibition of eukaryotic versus prokaryotic translation machinery.

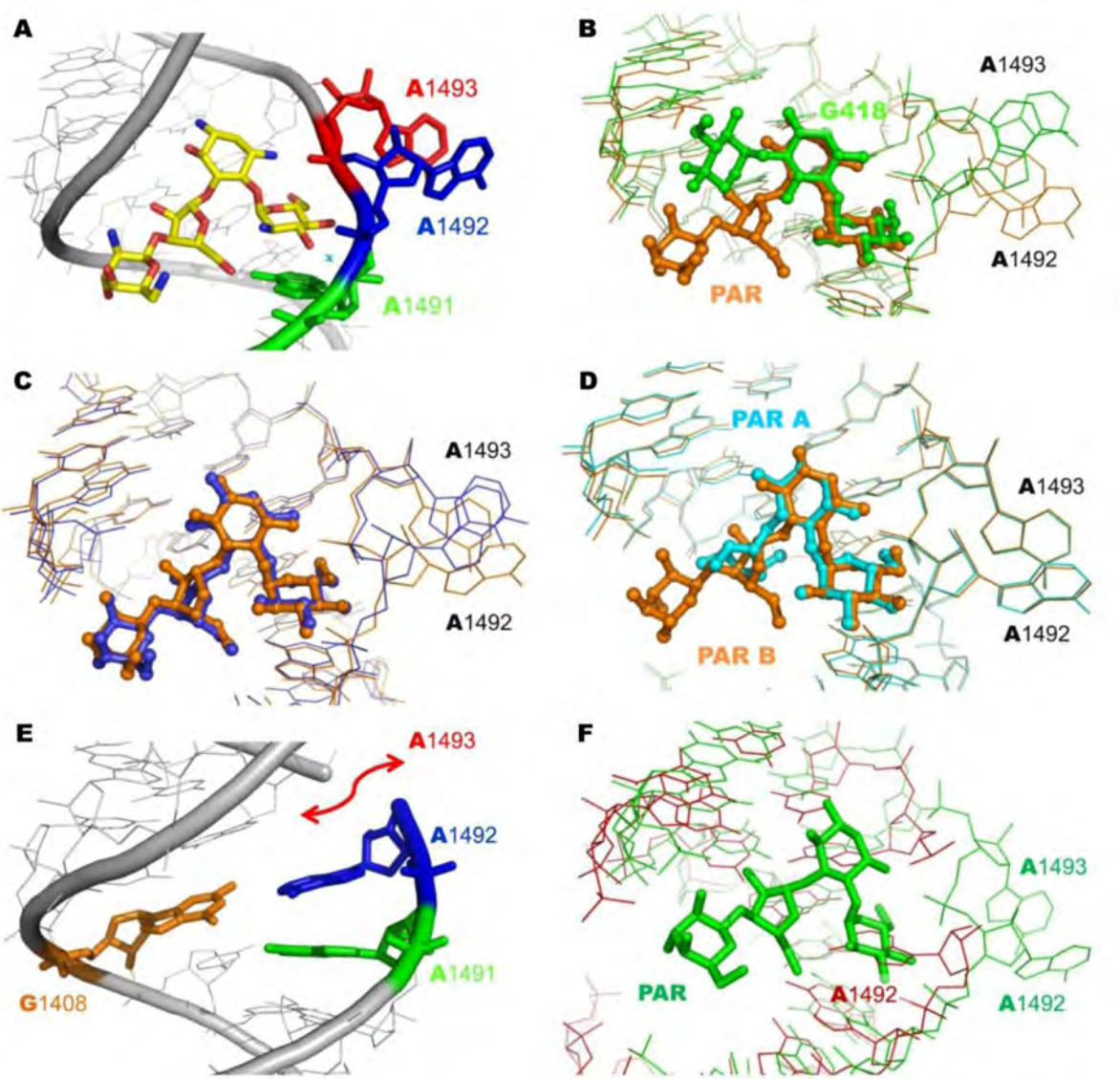

Figure 3. Visualization of the crystal structure of ligand-bound and ligand un-bound sites. (**A**) PAR (molecule B, yellow) bound to the leishmanial A-site rRNA model with A1491 highlighted in green, A1492 in blue and A1493 in red. (**B**) Superimposition of PAR (molecule B, orange) and G418 (green) bound to the leishmanial A-site. AGs are highlighted in ball-and-stick representations. Superimposition was performed using the PyMol software align algorithm using all atoms (rmsd, 0.7 Å). PDB ID codes are 4ZC7 and 4K32 for the PAR-Leish and G418-Leish structures, respectively. (**C**) Superimposition of PAR (ball-and-stick) bound to the bacterial (blue) and leishmanial (orange) A-sites (rmsd, 0.6 Å). PDB ID codes are 1J7T and 4ZC7 for the bacterial and *Leishmania* structures, respectively. (**D**) Superimposition of putative PAR binding modes to molecules A (cyan) and B (orange) representing the leishmanial ribosomal binding sites (rmsd, 0.3 Å). PDB ID code 4ZC7. (**E**) The ligand un-bound conformation. A1491 and A1492 are highlighted in green and blue, respectively. A1408 is highlighted in orange and A1493 location is indicated by a red arrow. (**F**) Superimposition of the bound (green) versus unbound (red) conformations in the PAR-Leish crystal structure. The superimposition was performed using an all-atom align command in PyMol (rmsd, 0.9 Å). PDB ID code 4ZC7.

In-silico exploration of ring III 5”-amino derivatives superiority in killing Leishmania

The selectivity of 5”-NH_2 modified derivatives towards eukaryotic ribosomes has previously been demonstrated for 4,5-disubstituted compounds that were specifically designed to target human ribosomes for the treatment of nonsense-mediated genetic disorders (16–20). However, structural evidence supporting such selectivity is still lacking and the only structures available are of natural and semi-synthetic derivatives in complex with their bacterial binding sites (30,31,36,40,47–49). No structures of 4,5-di-substituted AG derivatives are available for eukaryotic ribosomes and the current PAR-Leish structure is the first demonstration of 4,5-substituted derivatives binding modes. In contrast, the 4,6-di-substituted derivatives, such as G418, were shown to interact with both prokaryotic and eukaryotic ribosomes in a similar fashion (15,38,46,50). Comparison of crystal structures of PAR and G418 bound to the leishmanial ribosome target site indicates that while the structural rearrangements of the binding site upon binding of PAR are highly similar to those observed upon the

Table 1. *In vitro* inhibition of translation IC_{50} (μM)[a]

	Eukaryotes		Prokaryotes
	L. tarentolae[b]	*O. cuniculus*[c]	*E. coli*[d]
G418	0.19 ± 0.03	2 ± 0.3 (20)	0.009 ± 0.002 (20)
PAR	3.93 ± 0.39	57 ± 4 (17)	0.051 ± 0.005 (17)
1	>20	>200	0.44 ± 0.03
2	3.5 ± 0.5	31 ± 4 (17)	0.459 ± 0.053
3	0.4 ± 0.15	17 ± 0.6 (20)	1.2 ± 0.2 (20)
4	0.4 ± 0.03	1.5 ± 0.08 (16)	1.1 ± 0.2 (16)

[a]Each value represents the mean ± standard error of at least three independent experiments performed in duplicates.
[b]*L. tarentolate* S30 (reporter protein: EGFP).
[c]Rabbit reticulocytes S30 lysate for circular DNA (reporter protein: firefly luciferase).
[d]*E. coli* S30 lysate for circular DNA (reporter protein: firefly luciferase).

association with G418 (Figure 3B), the ligand's binding modes are largely different. The third ring of G418 is directed towards the strictly conserved region within the binding site, therefore limiting the differentiation of its binding between various ribosomal species (Supplementary Figure SIV, Table 1). In contrast, PAR's ring III can interact in several modes with some rather variable ribosomal regions (Supplementary Figure SIV), making it indeed an excellent target for chemical modifications to selectively target specific ribosomes.

In order to further understand the enhanced selectivity of 5"-amino modified 4,5-disubstitued AG derivatives to leishmanial ribosomes, compounds **1** and **2** were docked to their leishmanial putative binding site (Figure 4). In both structures rings I and II were stabilized and served as a conserved anchor that maintains the highly polar contacts with the rather conserved binding area. Ring I is stacked upon A1491 while maintaining two polar contacts with the eukaryotic conserved G1408 and ring II donating the conserved polar contacts via the amino groups located in positions 1 and 3. Interestingly, our docking results for the 5"-OH-containing compound **1** indicated a rather high flexibility of ring III (Figure 4A-B) which might explain the rather low inhibition profile of compound **1** when compared to PAR (Table 1). Surprisingly, the docking results for compound **2**, where an amino group is present at the same position of ring III, indicated a rather stable conformation where the 5"-NH_2 serves as a hydrogen bond donor for the O_6 G1408 keto-group (Figure 4C). This selective interaction might result from the positively charged 5"-NH_2 under physiological conditions; such increased polarity of 5"-NH_3^+ in compound **2** might enhance the bond strength to the O_6 keto-group of G1408 when compared to the hydrogen bonding donor characteristics of an 5"-OH in compound **1** (Figure 4A). Furthermore, in contrast to the 5"-OH (compound **1**) that could also maintain alternative interactions with the positively charged N_7 in A1491 (Figure 4B), the 5"-NH_2 (compound **2**) will avoid such interactions due to electrostatic repulsion and hence is selectively directed towards the eukaryotic specific G1408 (Figure 4C). Comparison between the calculated free binding energies for the two conformers of compound **1** and compound **2**, further supports these insights with the calculate value for compound **2** lower in 0.6 Kcal/mol even when compared to the most stable conformer of compound **1** (Supplementary Table S2).

A similar binding pattern of 5"-NH_2 in compound **2** cannot occur in prokaryotes, where an adenine instead of a guanine residue is located at position 1408 (Figure 4D). This is supported by a comparison between the previously reported structures of the natural three-ring scaffold ribostamicin, containing a 5"-OH group, and the 5"-NH_2-modified compound **2** bound to the bacterial A-sites (31). While the 5"-OH maintains an interaction with either the O_6 or N_7 group in G1491, the 5"-NH_2 is repulsed by the positively charged N_7 group and, given the lack of G1408, ring III of compound **2** does not maintain any type of interactions within the binding site (Figure 4E). These structural data on differential leishmanial versus prokaryotic selectivity of compounds **1** and **2** are further supported by the measured IC_{50} values in both systems, which displayed the increase by 1–2 orders of magnitude (Table 1 (16)).

Inhibition of Leishmania ribosome translation, and Leishmania growth in suspension and in infected macrophages by PAR and structurally related novel AGs

The structural and biochemical exploration of compounds' **1** and **2** ability to inhibit leishmanial ribosomes highlighted the importance of 4,5- rather than 4,6- derivatization of AGs for better selectivity, as well as the superiority of a 5"-NH_2 moiety in ring III over a 5"-OH moiety. Nevertheless, our *in vitro* studies indicated that compound **2** was as active as PAR in inhibiting leishmanial protein translation. Previous studies testing the efficacy of a series of compounds, all derived from compound **2**, have shown great promise in targeting human ribosomes for the treatment of genetic diseases (16,20). Two of these compounds (compounds **3** and **4**, Figure 1) demonstrated especially high selectivity to eukaryotic ribosomes as well as low mitoribosome interference (51) and improved cell toxicity profiles (16). The two compounds are structurally related to compound **2**, both containing a G418-like modified ring I with an additional chiral 6′-(*R*)-methyl group. Compound **4** is also installed with an additional chiral 5"-(*S*)-methyl moiety.

To evaluate the ability of these compounds to interfere with leishmanial translation and to inhibit parasite growth, a set of cell free assays were designed using extracts prepared from *L. tarentolae*. In addition, viability assays were performed using two *Leishmania* species. As indicated in Table 1, both synthetic derivatives were significantly better inhibitors of leishmanial translation when compared to PAR

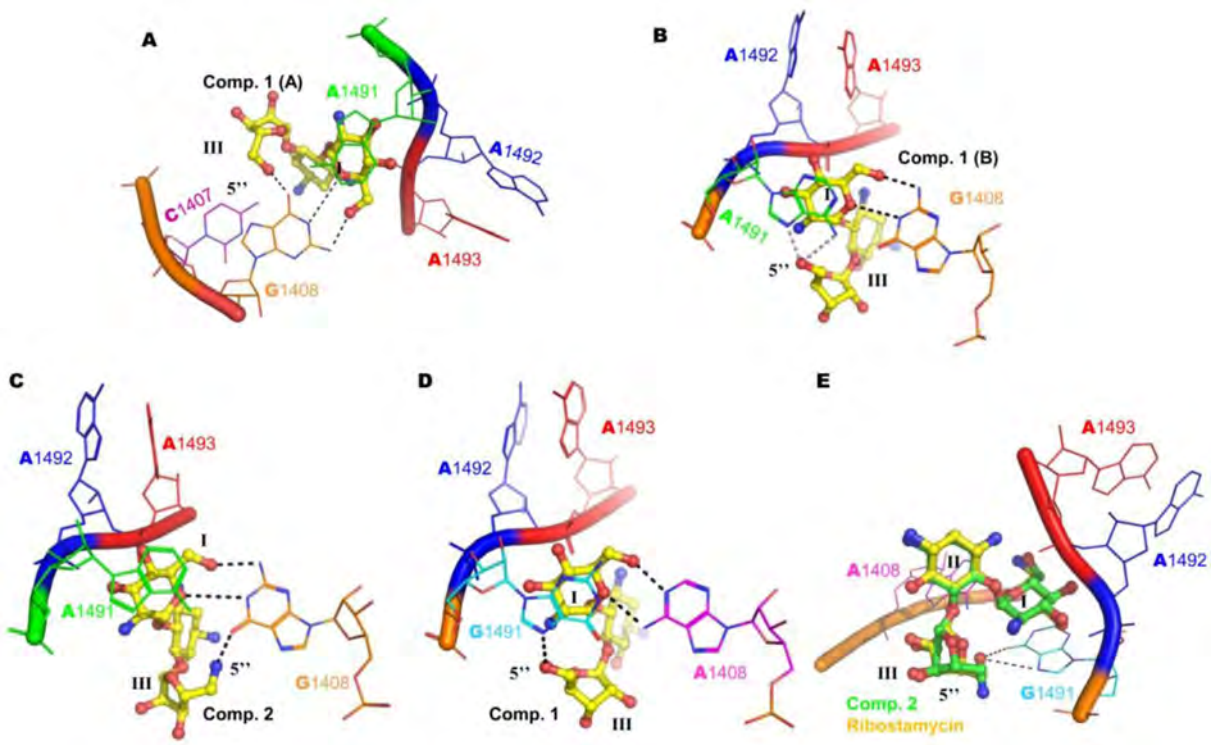

Figure 4. Modelling of compounds **1** and **2** to the leishmanial and bacterial ribosomes. (**A**-**B**) Various conformations obtained from compound **1** (5'' -OH) docking experiments to the leishmanial A-site. Unique conformers are marked as 1(A) and 1(B). (**C**). Alternate conformation of compound **2** (5'' -NH_2) docked to the leishmanial A-site. (**D**). Compound **1** docked to bacterial A-site. (**E**) Superimposition of crystal structures of ribostamicin (yellow) and compound **2** (green) bound to the bacterial A-site (PDB codes are 2ET5 and 2O3X, respectively). In all figures, aminoglycosides are represented in ball-and-stick and are highlighted in yellow, unless otherwise stated. The conserved adenine residues, A1492 and A1493, are indicated in blue and red, respectively. A1491 in *Leishmania* is marked in green; G1491 in bacteria is marked in cyan. G1408 in *Leishmania* is coloured orange and the A1408 in bacteria is pink. Rings I and III are marked in black Latin numbers, the 5'' position is indicated in black. Possible hydrogen bonds are drawn as black dashed lines, alternative bonds are also highlighted in black. Docking experiments were performed using the Autodock Vina package version 1.1.2 1. Figures were created using PyMol.

and compound **2** (IC_{50} values for PAR, compounds **2**, **3** and **4** are: 3.9, 3.5, 0.4 and 0.4 μM, respectively), and were in fact closer in their biological activities to G418 which is 20 times more potent in inhibiting leishmanial ribosomal translation than PAR. A similar trend was observed with compounds **3** and **4** in *Leishmania* viability assays using promastigotes from pathogenic species *L. major* and *L. donovani*, that cause CL and VL in humans, respectively (Figure 5A and B). These compounds showed better activity than PAR (LC_{50} values for *L. major* PAR = 31.4 ± 5.7 μM, **3** = 8.2 ± 1.5 μM and **4** = 5.9 ± 1.2 μM; for *L. donovani* PAR = 48.1 ± 5.8 μM, **3** = 37.2 ± 4.7 μM and **4** = 22.5 ± 2.2 μM). The trend observed between activity using the *in vitro* translation assay and *Leishmania* growth suggests that the mechanism of action of these compounds also involves inhibition of the parasite translational machinery upon exposure to AGs, and further emphasizes the importance of leishmanial ribosomal inhibition as a mechanism of action against *Leishmania*. The explanation for the derivatives' higher activity against *L. major* as compared to *L. donovani* is not clear, but different species of *Leishmania* vary in their sensitivity to AGs with *L. major* generally more sensitive to PAR and G418 than *L. donovani* (Figure 5 (15)). This variation might be explained in part by the differences in membrane glycoproteins and glycolipids, such as lipophosphoglycan and proteophosphoglycan, that differ between two species and might affect AG penetration (52).

We further evaluated the compounds potency as possible therapeutic agents for the treatment of leishmaniasis by determining their activity against intracellular *L. donovani* amastigotes in the infected THP-1 macrophage cell line (Figure 5C). Macrophages are the primary target of *Leishmania* in the host where the intracellular stage of the parasite, the stage responsible for disease, resides and multiples; and as such the investigation of AG activity in infected cells is of high importance. Parasite viability assays using infected macrophages indicated that both compounds were highly potent inhibitors of amastigote growth (LC_{50} compounds **3** and **4** = 16.6 ± 3.6 μM and 9.4 ± 2.6 μM, respectively) equal or better than PAR (LC_{50} = 16.3 ± 4.3 μM).

PAR semi-synthetic derivative 3 exhibits lower toxicity profile when compared to PAR

One of the major drawbacks limiting the clinical use of AGs is their irreversible ototoxicity. Hearing loss has been documented in 1 out of 5 patients over short courses of AG treatment (53), while severe ototoxic effects are recorded in more than 90% of the long-term treated patients (54). Re-

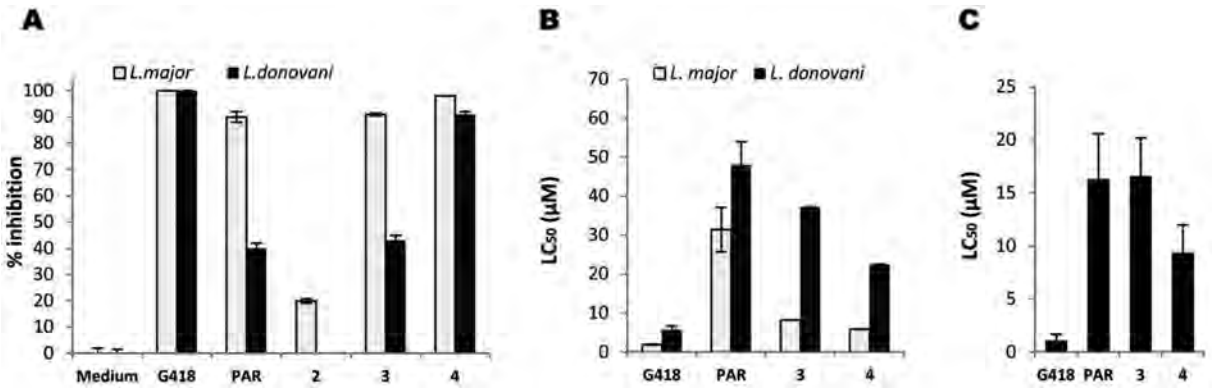

Figure 5. *In vitro* inhibition of *L. major* and *L. donovani* promastigote growth. (**A**) in the presence of a single dose (50 μM) of AGs. (**B**) LC_{50} values (50% growth inhibition) obtained from experiments with variable AG concentrations. (**C**). LC_{50} values for inhibition of *L. donovani* amastigote growth in THPI infected cells. All AGs tested inhibited *Leishmania* growth in a dose dependent manner.

cent studies have linked these adverse-effects to the limited selectivity of AGs to their targeted ribosome species and suggested that mitochondrial dysfunction plays a key role in AG-mediated ototoxicity (51,55,56). These studies also highlighted the mitochondrial protein synthesis machinery, and more precisely, the mitoribosome A-site (Supplementary Figure SIII), as the primary target affecting mitochondrial malfunction upon AG exposure; thus indicating the importance of cytoplasmic or bacterial ribosome selectivity over the mitoribosome to reduce AG-induced ototoxic effects (51).

In previous studies, compounds **3** and **4** were both shown to poorly inhibit mitoribosome translation (16), and also demonstrated reduced toxic effects on auditory hair cells in murine cochlear explants when compared to gentamicin (51,57). Compound **3** was also shown to have a better ototoxicity profile in guinea pigs *in-vivo* (51). However, due to the fact that these synthetic derivatives were initially designed for the treatment of genetic disorders, their recorded ototoxic effects were always compared to gentamicin, which was already in advanced clinical phases for the treatment of genetic disorders (57), or to the highly toxic G418 which was banned from clinical use due to its high acute and ototoxicity profile (51,57). Gentamicin was recently shown to lack an anti-leishmanial activity (15), and no comparable data on ototoxicity was available in regards to PAR. Therefore we compared the ototoxic potential of compounds **3** and **4** to PAR and G418 (Figure 6). Quantitative evaluation of auditory outer hair cells (OHC) along the entire length murine explants (Figure 6A) confirmed the high toxicity of G418, and also indicated that compound **3** showed less toxicity than PAR. Compound **4** exhibited a slightly enhanced toxicity as compared to PAR (IC^{Coch}_{50} PAR = 30 μM, **3** = 125 μM and **4** = 15 μM). The difference between compound **3** and PAR is illustrated by the pathology induced in the basal turn of the explants, the area most sensitive to aminoglycoside damage (Figure 6C). Incubations with 22 or 33 μM compound **3** left the morphology of OHC intact, but 22 μM PAR caused significant loss of OHC and at 33 μM PAR their complete destruction. A more rigorous test of an agent's potential suitability for clinical application is the assessment of ototoxicity *in vivo* (Figure 6B). Auditory performance in guinea pigs significantly deteriorated following 14 days of treatment with PAR, leading to large shifts of hearing thresholds similar to other clinically used AGs such as gentamicin and amikacin that are known to induce ototoxic side effects in 10 to 20% of patients receiving short-term treatment. This result correlates well with early studies in several animal models (58) and is consistent with reports of ototoxicity of PAR in clinical trials in India (2%) (7) and East Africa (59). In contrast, compound **3** did not significantly affect thresholds at a dose of 140 mg/kg (for 14 days); at such a dose, PAR already elevated thresholds by about 40 dB. The sum of these experiments clearly suggests an enhanced safety of compound **3** over PAR.

While studies on the effectiveness, formulation and pharmokinetics of the synthetic compound **3** in animal models and humans still need to be carried out, the low toxicity profile and high selectivity for eukaryotes makes compound **3** a suitable candidate to treat leishmaniasis. In CL, toxicity is less problematic as single lesions are generally treated topically, however in severe CL where multiple lesions are present, or in mucocutaneous leishmaniasis and VL where drugs are given systematically toxicity can be a serious problem. This fact coupled with the increasing use of PAR in mono- and combination drug therapy for VL highlights the need for new, safe and effective drugs. While the use of non-selective compounds, such as PAR, to treat CL could be useful since it would kill the parasite while simultaneously preventing bacterial infections, such compounds could also promote the development of bacterial resistance to PAR during treatment. The presence of resistant bacteria might then reduce drug efficacy against the parasites in the same lesions. On the other hand selectivity, in the treatment of VL, might be highly beneficial by avoiding microflora disruption upon IV administration, as well as diminishing the severe adverse side effects that might result from PAR administration. Finally further investigation into the mechanism of action of AG derivatives via ribosomal binding and inhibition of protein translation will lead to the development of new, safer and more effective inhibitors for these parasites.

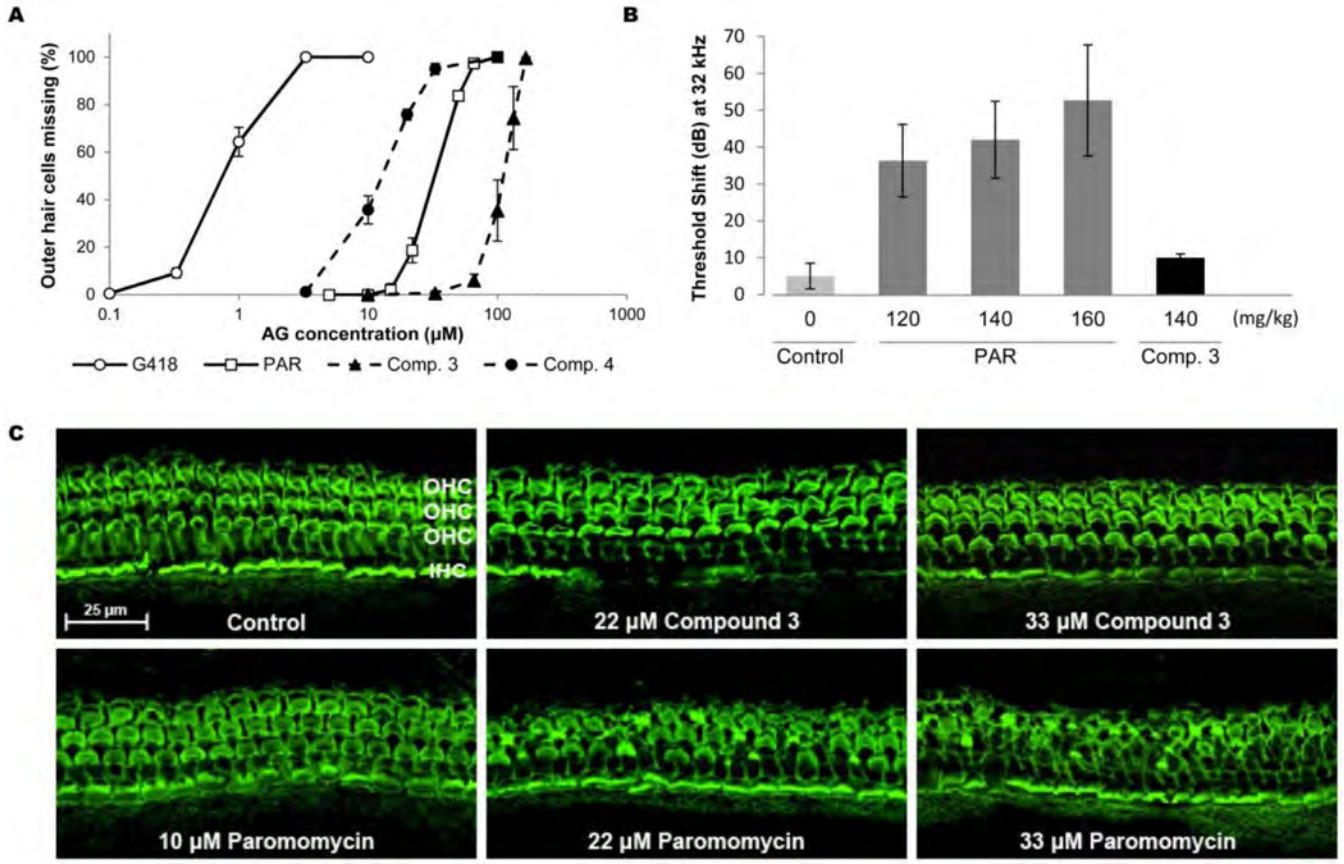

Figure 6. Aminoglycoside-induced hair cell death *in vitro* and ototoxicity *in-vivo*. (**A**) Organotypic cultures of the postnatal day 2–3 murine cochlea were exposed to various doses of AGs for 72 h and assessed for hair cell pathology. Hair cell loss was quantified along the entire length of the explant. Values are means of 3–5 replications per data point. (**B**) Guinea pigs were treated with s.c. injections of various dosages of PAR or compound **3**, or of saline (control) once daily for 14 d. Auditory thresholds were recorded by auditory brain stem responses (ABR) before and after the drug treatment, and threshold shifts caused by the treatment are plotted in dB. Data represent means ± SD, $n = 3$ per treatment. Data for compound **3** are from Shulman et al. (2014) (51) and are shown here for comparison. Significance of differences: PAR treatment at any concentration differs from control and from compound **3** ($P < 0.05$); compound **3** does not differ from controls. (**C**) Comparison of hair cell pathology. Representative samples from the dose-response experiments were taken from comparable areas of the basal turn of the cochlear explant. Staining for actin with rhodamine phalloidin shows the intact stereocilia and outline of three rows of outer and one row of inner hair cells in the 'Control' and in incubations with compound **3** at 22 μM and 33 μM and PAR 10 μM. PAR, however, causes partial destruction of outer hair cells at 22 μM and complete elimination of basal-turn outer hair cells at 33 μM.

SUMMARY AND CONCLUSIONS

Recent outbreaks of Leishmaniasis worldwide, along with a rather limited therapeutic arsenal and alarming levels of resistant parasite strains, highlight the need to identify novel therapeutic agents. A promising approach is the delineation of new cellular drug-targets through mechanistic studies. The leishmanial ribosome is one potential target of anti-leishmanial therapeutics, especially for derivatives belonging to the AG family.

Recent structural studies aimed at deciphering the mechanisms of AGs action against *Leishmania* provided important insights regarding those structural attributes important for AGs deferential activity against leishmmanial ribosomes. These studies highlighted di-substituted AGs with a paromamine-like structure, especially G418, as promising candidates that target leishmanial ribosomes and gave a structural explanation for the superiority of the 6′-OH group on AG ring I as compared to the 6′-NH_2 moiety (15). The studies revealed that the structural rearrangements of the leishmanial binding site upon G418 binding highly resemble the ones present in bacterial ribosomes and thus suggested its mechanism of action against *Leishmania* to be similar to AGs well documented mechanisms in bacteria. In addition, the authors raised two main concerns in regards to the use of G418 and similar derivatives in the treatment of leishmaniasis: the first was the lack of selectivity of natural derivatives such as G418 for leishmanial ribosomes and the second was regarding their high toxicity profile in humans.

The structural data presented in this work elucidate PAR binding modes to the *Leishmania* ribosomal A-site and highlight the importance of ring III, and in particular position 5", in determining AGs species-selectivity. These studies represent the first structural description of 4,5-disubstituted AGs binding modes to eukaryotic ribosomes and have additional implications regarding the molecular attributes governing their species selectivity. Structural and biochemical analysis of a series of both natural and synthetic AGs further stresses the importance of position 5" for species-specificity and emphasizes the superiority of 5"-NH_2 moiety over 5"-OH moiety in 4,5-disubstituted AGs

for the enhanced binding and selective action towards leishmanial versus prokaryotic ribosomes. Two of the semi-synthetic derivatives, compounds **3** and **4**, tested as part of this study, were identified as potentially potent candidates for the treatment of leishmaniasis. The low ototoxicity of compound **3**, eliminating an important drawback that limits clinical use of AGs, further highlights this semi-synthetic derivative as promising therapeutic candidate for the treatment of VL. The structural and biochemical data presented here will be valuable in the rational design and development of new derivatives as potential therapeutic agents for the treatment of leishmaniasis.

SUPPLEMENTARY DATA

Supplementary Data are available at NAR Online.

ACKNOWLEDGEMENT

We gratefully thank the staff of beamline 14–4, ESRF, for provision of synchrotron radiation facilities and assistance. A special thank is for the great team of the 7th CCP4/APS crystallography school, held on July 2014 at the Advanced Photon Source (APS) synchrotron site at Argonne National Laboratory, for their helpful advices on crystal data analysis. The authors also wish to thank Dr Jing Xie and Ann Kendall (University of Michigan) for their contributions to the study. V.B. acknowledges the financial support by the Center of Absorption in Science, the Ministry of Immigration Absorption and the Ministry of Science and Technology, Israel (Kamea Program).

FUNDING

NIH/NIGMS [1 R01 GM094792-01 A1 to T.B. and J.S.]; Technion Fund for Applied Research [2017794 to T.B.]; Bill and Melinda Gates Foundation [OPPGH5336 to C.L.J.]. C.L.J. holds the Michael and Penny Feiwel Chair in Dermatology. Funding for open access charge: Technion Fund for Applied Research [2017794 to T.B.].

Conflict of interest statement. Timor Baasov declares that the compounds 2, 3 and 4 discussed in this publication are subject to license agreement granted to a commercial third party.

REFERENCES

1. Second WHO report on neglecteg tropical diseases. (2013) pp. 67–71.
2. Moore,T.A. (2005) Agents used to treat infections due to parasites and pneumocystis. In: Kasper,DL (ed). *Harrison's Principles of Internal Medicine*, 16th edn. Mc Graw Hill, Vol. **1**, pp. 1202–1214.
3. Neal,R.A. (1968) The effect of antibiotics of the neomycin group on experimental cutaneous leishmaniasis. *Ann. Trop. Med. Parasitol.*, **62**, 54–62.
4. Ben,S.A., Ben,M.N., Guedri,E., Zaatour,A., Ben,A.N., Bettaieb,J., Gharbi,A., Belhadj,H.N., Boukthir,A., Chlif,S. *et al.* (2013) Topical paromomycin with or without gentamicin for cutaneous leishmaniasis. *N. Engl. J. Med.*, **368**, 524–532.
5. Lecoeur,H., Buffet,P.A., Milon,G. and Lang,T. (2010) Early curative applications of the aminoglycoside WR279396 on an experimental *Leishmania* major-loaded cutaneous site do not impair the acquisition of immunity. *Antimicrob. Agents Chemother.*, **54**, 984–990.
6. El-On,J., Weinrauch,L., Livshin,R., Even-Paz,Z. and Jacobs,G.P. (1985) Topical treatment of recurrent cutaneous leishmaniasis with ointment containing paromomycin and methylbenzethonium chloride. *Br. Med. J. (Clin. Res. Ed.)*, **291**, 704–705.
7. Sundar,S., Jha,T.K., Thakur,C.P., Sinha,P.K. and Bhattacharya,S.K. (2007) Injectable paromomycin for Visceral leishmaniasis in India. *N. Engl. J. Med.*, **356**, 2571–2581.
8. WHO model list of essential medicines. (2007). 17th edn. 15.
9. Sundar,S. and Chakravarty,J. (2013) Leishmaniasis: an update of current pharmacotherapy. *Expert. Opin. Pharmacother.*, **14**, 53–63.
10. Sundar,S., Sinha,P.K., Rai,M., Verma,D.K., Nawin,K., Alam,S., Chakravarty,J., Vaillant,M., Verma,N., Pandey,K. *et al.* (2011) Comparison of short-course multidrug treatment with standard therapy for visceral leishmaniasis in India: an open-label, non-inferiority, randomised controlled trial. *Lancet*, **377**, 477–486.
11. Maarouf,M., de,K.Y., Brown,S., Petit,P.X. and Robert-Gero,M. (1997) In vivo interference of paromomycin with mitochondrial activity of *Leishmania*. *Exp. Cell Res.*, **232**, 339–348.
12. Fernandez,M.M., Malchiodi,E.L. and Algranati,I.D. (2011) Differential effects of paromomycin on ribosomes of *Leishmania* mexicana and mammalian cells. *Antimicrob. Agents Chemother.*, **55**, 86–93.
13. Hobbie,S.N., Kaiser,M., Schmidt,S., Shcherbakov,D., Janusic,T., Brun,R. and Bottger,E.C. (2011) Genetic reconstruction of protozoan rRNA decoding sites provides a rationale for paromomycin activity against *Leishmania* and *Trypanosoma*. *PLoS Negl. Trop. Dis.*, **5**, e1161.
14. Maarouf,M., Lawrence,F., Croft,S.L. and Robert-Gero,M. (1995) Ribosomes of *Leishmania* are a target for the aminoglycosides. *Parasitol. Res.*, **81**, 421–425.
15. Shalev,M., Kondo,J., Kopelyanskiy,D., Jaffe,C.L., Adir,N. and Baasov,T. (2013) Identification of the molecular attributes required for aminoglycoside activity against *Leishmania*. *Proc. Natl. Acad. Sci. U.S.A.*, **110**, 13333–13338.
16. Kandasamy,J., Atia-Glikin,D., Shulman,E., Shapira,K., Shavit,M., Belakhov,V. and Baasov,T. (2012) Increased selectivity toward cytoplasmic versus mitochondrial ribosome confers improved efficiency of synthetic aminoglycosides in fixing damaged genes: a strategy for treatment of genetic diseases caused by nonsense mutations. *J. Med. Chem.*, **55**, 10630–10643.
17. Kondo,J., Hainrichson,M., Nudelman,I., Shallom-Shezifi,D., Barbieri,C.M., Pilch,D.S., Westhof,E. and Baasov,T. (2007) Differential selectivity of natural and synthetic aminoglycosides towards the eukaryotic and prokaryotic decoding A sites. *Chembiochem.*, **8**, 1700–1709.
18. Nudelman,I., Rebibo-Sabbah,A., Shallom-Shezifi,D., Hainrichson,M., Stahl,I., Ben-Yosef,T. and Baasov,T. (2006) Redesign of aminoglycosides for treatment of human genetic diseases caused by premature stop mutations. *Bioorg. Med. Chem. Lett.*, **16**, 6310–6315.
19. Nudelman,I., Rebibo-Sabbah,A., Cherniavsky,M., Belakhov,V., Hainrichson,M., Chen,F., Schacht,J., Pilch,D.S., Ben-Yosef,T. and Baasov,T. (2009) Development of novel aminoglycoside (NB54) with reduced toxicity and enhanced suppression of disease-causing premature stop mutations. *J. Med. Chem.*, **52**, 2836–2845.
20. Nudelman,I., Glikin,D., Smolkin,B., Hainrichson,M., Belakhov,V. and Baasov,T. (2010) Repairing faulty genes by aminoglycosides: development of new derivatives of geneticin (G418) with enhanced suppression of diseases-causing nonsense mutations. *Bioorg. Med. Chem.*, **18**, 3735–3746.
21. Berger,I., Kang,C.H., Sinha,N., Wolters,M. and Rich,A. (1996) A highly efficient 24-condition matrix for the crystallization of nucleic acid fragments. *Acta Crystallogr. D Biol. Crystallogr.*, **52**, 465–468.
22. Kabsch,W. (2010) XDS. *Acta Crystallogr. D Biol. Crystallogr.*, **66**, 125–132.
23. Adams,P.D., Afonine,P.V., Bunkoczi,G., Chen,V.B., Davis,I.W., Echols,N., Headd,J.J., Hung,L.W., Kapral,G.J., Grosse-Kunstleve,R.W. *et al.* (2010) PHENIX: a comprehensive Python-based system for macromolecular structure solution. *Acta Crystallogr. D Biol. Crystallogr.*, **66**, 213–221.
24. Emsley,P. and Cowtan,K. (2004) Coot: model-building tools for molecular graphics. *Acta Crystallogr. D Biol. Crystallogr.*, **60**, 2126–2132.

25. The PyMol Molecular Graphics System. (2010) Schrödinger, LLC, V.1.5.0.4.S.L.
26. Leatherbarrow,R.J. (2001) *GraFit*. Erithacus Software Ltd. Horley, Vol. **5**.
27. Trott,O. and Olson,A.J. (2010) AutoDock Vina: improving the speed and accuracy of docking with a new scoring function, efficient optimization, and multithreading. *J Comput. Chem.*, **31**, 455–461.
28. Morris,G.M., Huey,R., Lindstrom,W., Sanner,M.F., Belew,R.K., Goodsell,D.S. and Olson,A.J. (2009) AutoDock4 and AutoDockTools4: Automated docking with selective receptor flexibility. *J Comput. Chem.*, **30**, 2785–2791.
29. Aghdam,E.M., Hejazi,M.S. and Barzegar,A. (2014) Riboswitches as potential targets for aminoglycosides in comparing with rRNA molecules: in silico study. *Microb. Biochem. Technol.*, **9**, S9.
30. Francois,B., Szychowski,J., Adhikari,S.S., Pachamuthu,K., Swayze,E.E., Griffey,R.H., Migawa,M.T., Westhof,E. and Hanessian,S. (2004) Antibacterial aminoglycosides with a modified mode of binding to the ribosomal-RNA decoding site. *Angew. Chem. Int. Ed. Engl.*, **43**, 6735–6738.
31. Francois,B., Russell,R.J., Murray,J.B., Aboul-ela,F., Masquida,B., Vicens,Q. and Westhof,E. (2005) Crystal structures of complexes between aminoglycosides and decoding A site oligonucleotides: role of the number of rings and positive charges in the specific binding leading to miscoding. *Nucleic Acids Res.*, **33**, 5677–5690.
32. Hermann,T., Tereshko,V., Skripkin,E. and Patel,D.J. (2007) Apramycin recognition by the human ribosomal decoding site. *Blood Cells Mol. Dis.*, **38**, 193–198.
33. Kondo,J., Francois,B., Urzhumtsev,A. and Westhof,E. (2005) Crystallographic studies of Homo sapiens ribosomal decoding A site complexed with aminoglycosides. *Nucleic Acids Symp. Ser. (Oxf.)*, **49**, 253–254.
34. Kondo,J., Francois,B., Urzhumtsev,A. and Westhof,E. (2006) Crystal structure of the Homo sapiens cytoplasmic ribosomal decoding site complexed with apramycin. *Angew. Chem. Int. Ed. Engl.*, **45**, 3310–3314.
35. Kondo,J., Pachamuthu,K., Francois,B., Szychowski,J., Hanessian,S. and Westhof,E. (2007) Crystal structure of the bacterial ribosomal decoding site complexed with a synthetic doubly functionalized paromomycin derivative: a new specific binding mode to an a-minor motif enhances in vitro antibacterial activity. *ChemMedChem*, **2**, 1631–1638.
36. Vicens,Q. and Westhof,E. (2001) Crystal structure of paromomycin docked into the eubacterial ribosomal decoding A site. *Structure*, **9**, 647–658.
37. Vicens,Q. and Westhof,E. (2002) Crystal structure of a complex between the aminoglycoside tobramycin and an oligonucleotide containing the ribosomal decoding a site. *Chem. Biol.*, **9**, 747–755.
38. Vicens,Q. and Westhof,E. (2003) Crystal structure of geneticin bound to a bacterial 16S ribosomal RNA A site oligonucleotide. *J Mol. Biol.*, **326**, 1175–1188.
39. Carter,A.P., Clemons,W.M., Brodersen,D.E., Morgan-Warren,R.J., Wimberly,B.T. and Ramakrishnan,V. (2000) Functional insights from the structure of the 30S ribosomal subunit and its interactions with antibiotics. *Nature*, **407**, 340–348.
40. Ogle,J.M., Brodersen,D.E., Clemons,W.M. Jr, Tarry,M.J., Carter,A.P. and Ramakrishnan,V. (2001) Recognition of cognate transfer RNA by the 30S ribosomal subunit. *Science*, **292**, 897–902.
41. Ogle,J.M., Murphy,F.V., Tarry,M.J. and Ramakrishnan,V. (2002) Selection of tRNA by the ribosome requires a transition from an open to a closed form. *Cell*, **111**, 721–732.
42. Ogle,J.M. and Ramakrishnan,V. (2005) Structural insights into translational fidelity. *Annu. Rev. Biochem.*, **74**, 129–177.
43. Kondo,J., Urzhumtsev,A. and Westhof,E. (2006) Two conformational states in the crystal structure of the Homo sapiens cytoplasmic ribosomal decoding A site. *Nucleic Acids Res.*, **34**, 676–685.
44. Kondo,J. and Westhof,E. (2008) The bacterial and mitochondrial ribosomal A-site molecular switches possess different conformational substates. *Nucleic Acids Res.*, **36**, 2654–2666.
45. Simonsen,K.B., Ayida,B.K., Vourloumis,D., Takahashi,M., Winters,G.C., Barluenga,S., Qamar,S., Shandrick,S., Zhao,Q. and Hermann,T. (2002) Novel paromamine derivatives exploring shallow-groove recognition of ribosomal-decoding-site RNA. *Chembiochem*, **3**, 1223–1228.
46. Garreau de,L.N., Prokhorova,I., Holtkamp,W., Rodnina,M.V., Yusupova,G. and Yusupov,M. (2014) Structural basis for the inhibition of the eukaryotic ribosome. *Nature*, **513**, 517–522.
47. Kondo,J., Koganei,M., Maianti,J.P., Ly,V.L. and Hanessian,S. (2013) Crystal structures of a bioactive 6'-hydroxy variant of sisomicin bound to the bacterial and protozoal ribosomal decoding sites. *ChemMedChem*, **8**, 733–739.
48. Maianti,J.P., Kanazawa,H., Dozzo,P., Matias,R.D., Feeney,L.A., Armstrong,E.S., Hildebrandt,D.J., Kane,T.R., Gliedt,M.J., Goldblum,A.A. *et al.* (2014) Toxicity modulation, resistance enzyme evasion, and A-site X-ray structure of broad-spectrum antibacterial neomycin analogs. *ACS Chem. Biol.*, **9**, 2067–2073.
49. Szychowski,J., Kondo,J., Zahr,O., Auclair,K., Westhof,E., Hanessian,S. and Keillor,J.W. (2011) Inhibition of aminoglycoside-deactivating enzymes APH(3′)-IIIa and AAC(6′)-Ii by amphiphilic paromomycin O2"-ether analogues. *ChemMedChem*, **6**, 1961–1966.
50. Kondo,J. (2012) A structural basis for the antibiotic resistance conferred by an A1408G mutation in 16S rRNA and for the antiprotozoal activity of aminoglycosides. *Angew. Chem. Int. Ed. Engl.*, **51**, 465–468.
51. Shulman,E., Belakhov,V., Wei,G., Kendall,A., Meyron-Holtz,E.G., Ben-Shachar,D., Schacht,J. and Baasov,T. (2014) Designer aminoglycosides that selectively inhibit cytoplasmic rather than mitochondrial ribosomes show decreased ototoxicity: a strategy for the treatment of genetic diseases. *J Biol. Chem.*, **289**, 2318–2330.
52. Jhingran,A., Chawla,B., Saxena,S., Barrett,M.P. and Madhubala,R. (2009) Paromomycin: uptake and resistance in *Leishmania donovani*. *Mol. Biochem. Parasitol.*, **164**, 111–117.
53. Forge,A. and Schacht,J. (2000) Aminoglycoside antibiotics. *Audiol. Neurootol.*, **5**, 3–22.
54. Duggal,P. and Sarkar,M. (2007) Audiologic monitoring of multi-drug resistant tuberculosis patients on aminoglycoside treatment with long term follow-up. *BMC Ear Nose Throat Disord.*, **7**, 5.
55. Hobbie,S.N., Akshay,S., Kalapala,S.K., Bruell,C.M., Shcherbakov,D. and Bottger,E.C. (2008) Genetic analysis of interactions with eukaryotic rRNA identify the mitoribosome as target in aminoglycoside ototoxicity. *Proc. Natl. Acad. Sci. U.S.A.*, **105**, 20888–20893.
56. Matt,T., Ng,C.L., Lang,K., Sha,S.H., Akbergenov,R., Shcherbakov,D., Meyer,M., Duscha,S., Xie,J., Dubbaka,S.R. *et al.* (2012) Dissociation of antibacterial activity and aminoglycoside ototoxicity in the 4-monosubstituted 2-deoxystreptamine apramycin. *Proc. Natl. Acad. Sci. U.S.A.*, **109**, 10984–10989.
57. Xue,X., Mutyam,V., Tang,L., Biswas,S., Du,M., Jackson,L.A., Dai,Y., Belakhov,V., Shalev,M., Chen,F. *et al.* (2014) Synthetic aminoglycosides efficiently suppress cystic fibrosis transmembrane conductance regulator nonsense mutations and are enhanced by ivacaftor. *Am. J Respir. Cell Mol. Biol.*, **50**, 805–816.
58. Manzo,E. and Mea,O. (1967) [Ototoxicity of aminosidine. II. Histological studies in the guinea pig]. *Arch. Ital. Laringol.*, **75**, 189–199.
59. Musa,A., Khalil,E., Hailu,A., Olobo,J., Balasegaram,M., Omollo,R., Edwards,T., Rashid,J., Mbui,J., Musa,B. *et al.* (2012) Sodium stibogluconate (SSG) & paromomycin combination compared to SSG for visceral leishmaniasis in East Africa: a randomised controlled trial. *PLoS Negl. Trop. Dis.*, **6**, e1674.